Functionally graded electrospun polycaprolactone and β-tricalcium phosphate nanocomposites for tissue engineering applications

Cevat Erisken, Dilhan M. Kalyon*, Hongjun Wang

Chemical, Biomedical and Materials Engineering Department, Stevens Institute of Technology, Hoboken, NJ 07030, USA

ABSTRACT

Fabricating functionally graded scaffolds from biodegradable polymers to enable the mimicking of native tissue is an important challenge. Here we demonstrate the fabrication and utilization of functionally graded non-woven meshes of polycaprolactone incorporated with tricalcium phosphate nanoparticles using a new hybrid twin-screw extrusion/electrospinning (TSEE) process, which allows the time-dependent feeding of various solid and liquid ingredients and their melting, dispersion, deaeration and pressurization together with electrospinning within the confines of a single process. Using this hybrid method, the concentration of tricalcium phosphate nanoparticles could be tailored to vary in a targeted/controlled manner between the two surfaces of the scaffold mesh. The graded scaffolds were seeded and cultured with mouse preosteoblast cells (MC3T3-E1). Within 4 weeks, the tissue constructs revealed the formation of continuous gradations in extracellular matrix with various markers including collagen synthesis and mineralization, akin to the type of variations observed in the typical bone-cartilage interface in terms of the distributions of concentration of Ca particles and of mechanical properties associated with this. The demonstrated hybrid method should allow much better control of the distributions of various ingredients, including the concentrations of drugs/growth factors, as well as the porosity, mechanical property, wettability, biodegradation rate distributions in tissue engineering scaffolds, aiming to mimic the elegant complex distributions found in native tissue.

© 2008 Elsevier Ltd. All rights reserved.

1. Introduction

Fabrication of biodegradable constructs which are functionally graded, especially in terms of porosity and composition distributions, to serve as realistic scaffolds that can lead to the mimicking of the complex spatial distributions of the composition, structure, and functionality of native tissues, is the ultimate objective of tissue engineering. For example, the microstructure of the bone tissue (which is a two-phase porous composite comprised mainly of calcium phosphate and collagen) is complicated by the presence of spatial differences in the orientations as well as the concentrations of its mineral and organic constituents [1,2]. Especially, at the bone-cartilage interface both the concentrations and the orientations of the calcium phosphate mineral particles vary in the direction normal to the axis of the interface [2–4]. Due to such hierarchical complexities, the engineering of a fully functional bone tissue still remains elusive, despite the excellent progress achieved up to date [5–9]. The typical composite scaffold consists of a biodegradable polymer homogeneously incorporated

with various additives including tricalcium phosphate [10,11], hydroxyapatite [12,13], calcium carbonate [14,15], carbon nanotubes [16,17], hydrogels [18] and proteins [19]. The preparation of such composite scaffolds currently relies on conventional techniques such as salt leaching, gas foaming, 3D printing, and electrospinning.

Obviously, the engineering of complex tissues need to utilize not homogeneous scaffolds but graded scaffolds, which can introduce the "establishment of compositional gradients and subcompartments, temporal changes and the use of cells to drive tissue morphogenesis" [20]. For example, one possible approximation to the graded compositional structure of bone has been attempted upon the fabrication of individual sheets of polycaprolactone and hydroxyapatite, collagen and hydroxyapatite, and polycaprolactone, collagen and hydroxyapatite separately and followed by the uniaxial pressing of the sheets into a consolidated pellet [21]. Schaefer et al. [22] prepared two individual sheets consisting of polyglycolic acid and poly-lactic-co-glycolic acid (PLGA) and then seeded chondrocytes and periosteal cells on them separately and then sutured the two constructs after 1 week of culture period. Gao et al. [23] prepared sheets of spongy hyaluronan and porous calcium phosphate and then joined them using a fibrin sealant. Spalazzi et al. [24] prepared three individual sheets composed of

---

PLGA and PLGA incorporated with bioactive glass and then sintered them together.

In the area of conventional electrospinning the sequential electrospinning of multiple sheets, each composed of a biodegradable polymer with various ingredients, and then their subsequent joining together is used to emulate the formation of distinct layers within a scaffold. Examples include the sequential electrospinning of a pure gelatin sheet crosslinked with a 20% hydroxyapatite incorporated gelatin [12]; a gelatin and elastin sheet followed by electrospinning of a sheet of elastin, gelatin and polyglyconate, which in turn was followed by a sheet of polyglyconate incorporated with gelatin [25]; and poly (3-hydroxybutyrate-co-4-hydroxybutyrate) and fluoroapatite with seven different concentration ratios [26]. Obviously, the labor-intensive generation of such scaffolds upon sequential electrospinning of multiple layers with differing compositions still involves the step changes in composition as one moves from one layer to another on one hand and suffers from the well-known restrictions and limitations of the conventional electrospinning process including, for example, the inability to keep rigid particles homogeneously suspended in the polymeric solution and the inability to prevent the agglomeration of the particles and especially nanoparticles during the course of the electrospinning process on the other.

A hybrid twin-screw-extrusion/electrospinning (TSEE) process was recently developed to enable the carrying out of multiple unit operations within the confines of a single apparatus including solids conveying, melting, temperature control, distributive and dispersive mixing of particles and nanoparticles, deaeration and electrospinning of nanofibrous membranes [27]. However, one important integral capability of the process, i.e., the feeding of solid and liquid ingredients in a time-dependent fashion to allow the generation of continuous spatial gradations in composition and porosity of electrospun nanofibrous membranes was not previously demonstrated. Here, this ability to generate spatially varying continuous compositional and porosity gradations to achieve 3D electrospun nanofibrous and nanocomposite biomimetic scaffolds is demonstrated and applied to the area of bone tissue regeneration, especially towards the controlled formation of the bone-cartilage interface.

2. Materials and methods

2.1. Materials

The ε-polycaprolactone (PCL) with a number average, M_n, molecular weight of 80,000 and β-tricalcium phosphate (β-TCP) nanoparticles were procured from Sigma-Aldrich (Saint Louis, MO). The particle diameter of β-TCP was measured to range between 50 nm and 2.5 μm. The dichloromethane (DCM) solvent was obtained from Pharmco (Brookfield, CT).

2.2. The hybrid twin-screw extrusion/electrospinning (TSEE) process for scaffold fabrication

The hybrid twin-screw extrusion/electrospinning (TSEE) process consists of a twin-screw extruder with fully intermeshing and co-rotating screws (Material Processing & Research, Inc., Hackensack, NJ) integrated with the electrospinning process [27]. The spinneret die with multi-channels for flow and shaping is connected to a high-voltage supply that is capable of generating DC voltages up to 30 kV. Injection ports and other feed ports in the barrel of the extruder enable the introduction of various liquid and solid ingredients/additives simultaneously with their flow rates varying in a time-dependent fashion to generate compositional and porosity variations in the electrospun non-woven meshes. The screw sections can be configured [28] to allow different operations like conveying, melting, mixing, shaping, and devolatilization to occur simultaneously. The dispersive mixing capability of the screws can also be tailored by using combinations of kneading discs with fully-flighted elements, staggered at the desired stagger angle and direction (kneading discs) or at any pitch (fully-flighted screw elements). The ability to introduce various ingredients of multiple formulations in a time-dependent fashion during electrospinning is a major advantage and enables manufacture of spatially graded electrospun membranes on a reproducible basis to thus eliminate one of the major drawbacks of the conventional electrospinning process.

The special design feature of the screws is the availability of reversely configured kneading blocks, i.e., lenticular discs staggered at an angle, to enable the application of relatively high shearing stresses especially suitable to break up the agglomerates of nanoparticles that need to be incorporated into the biodegradable polymeric matrix. This is a feature that would be totally lacking in the conventional electrospinning process, where the solution is mechanically displaced with a plunger/ram and uncontrolled migration/sedimentation of various ingredients is encountered. The presence of tight clearances between the screws and the barrel, and between the screws contributes to the dispersion capability of the process during conveying/melting/pumping/devolatilization, where the dispersive mixing and associated break up of the agglomerates arise due to the repeated passage of the suspension through small gaps, where relatively high shearing stresses are applied. The fully-intermeshing and self-swiping features of the co-rotating screws facilitate effective distributive mixing of the ingredients.

The operation of the twin-screw extruder (dual drive, i.e., could be hydraulically or servo-driven) was controlled by the aid of a computerized field-point based data acquisition/process control system. The unit has the capability to control temperatures over three different and separate heat transfer zones, which is again not possible in conventional electrospinning. The screw configuration was selected to generate three consecutive mixing zones, two of which were sealed with reversely staggered kneading discs and the third sealed with the die, to generate partially full sections in the extruder. This enables the break down of the continuity of the feed streams at intervals, and thus prevents the charges from reaching relatively long distances. The split die was designed/manufactured to allow multiple apertures, i.e., multiple fibers but only one aperture was used in the study.

For the demonstration study polycaprolactone was dissolved in dichloromethane (DCM) at a ratio of 12/100 (g/ml). The PCL/DCM solution was fed through one of the injection points into the first mixing zone of the extruder where β-TCP nanoparticles were also introduced from another injection point. Prior to the onset of the voltage to initiate the electrospinning process, there were no flow instabilities, which are frequently observed in the extrusion of polymeric melts and solutions [29]. The ability to control the feed rates of the PCL/DCM solution and β-TCP nanoparticles in a time-dependent fashion enabled the generation of continuously varying β-TCP concentrations in the non-woven mesh in the range of 0–15% by weight as the suspension was electrospun into nanofibers. The process allowed the generation of a linear concentration gradient of the TCP nanoparticles between the two surfaces of the meshes. To study the effect of β-TCP concentration on MC3T3-E1 cell attachment and growth rate, as well as on the mechanical properties of the composite mesh, a PCL-β-TCP mesh containing a constant 15% concentration of β-TCP by weight and pure PCL meshes were also fabricated under similar processing conditions.

2.3. Characterization of scaffolds

The diameter, morphology, and surface properties of the electrospun fibers were documented using a LEO Gemini 982 scanning electron microscopy. The weight fraction of β-TCP contained in the electrospun PCL-β-TCP non-woven meshes was validated by using a thermo-gravimetric analysis apparatus (TGA-Q50, TA Instruments of New Castle, Delaware) upon heating from 25 to 550 °C at 15 °C/min under N_2. The tensile properties of PCL and PCL-β-TCP composite meshes were characterized using a Rheometric Scientific Dynamic Mechanical Analyzer at a crosshead speed of 0.01 mm min^{-1} at 25 °C. The compression tests of PCL-β-TCP composite discs were performed using a Rheometric Scientific ARES Rheometer (currently TA Instruments) at a crosshead speed of 0.1 mm min^{-1} in a phosphate buffered saline (PBS) environment at 37 °C.

2.4. Proliferation of MC3T3-E1 cells on pure PCL and PCL-β-TCP scaffolds

In the first part of the study pure PCL and PCL-β-TCP scaffolds were individually prepared and subjected to cell proliferation studies. Electrospun PCL and PCL-β-TCP (containing 15% β-TCP) non-woven meshes were individually prepared and were then punched into 8.6 mm circular discs with 0.35–0.40 mm thickness. They were kept under vacuum until use. The discs were sterilized upon multiple immersions into 70% ethanol and then a PBS solution. To facilitate cell attachment the discs were then immersed in complete medium (see below) for 2 h at 37 °C and 5% CO$_2$. The MC3T3-E1 mouse preosteoblast cells from bone-calvaria (ATCC, Manassas, VA) were cultured in complete medium containing Minimum Essential Medium, Alpha 1X (Cellgro, Manassas, VA) supplemented with fetal bovine serum (Invitrogen, Carlsbad, CA) and penicillin/streptomycin (1/0.1/0.01 volume ratio, respectively) until 80% confluency before use. The preosteoblast cells were then detached with 0.25% Trypsin EDTA (Invitrogen, Carlsbad, CA), centrifuged, and resuspended in complete medium for use.

The cells were seeded onto the scaffolds placed in a 24 well plate (Corning, NY) at a density of 20,000 cells/cm^2. A total of 1 mL of complete medium was added to immerse the scaffolds completely followed by the culturing of the cells in an incubator at 37 °C and 5% CO$_2$. A similar number of cells were also seeded on polystyrene surfaces, as controls. The samples were harvested after 24, 72, and 120 h and the proliferation rates were determined using MTT assay. The attachment and morphology of the cells were assessed using polarized light microscopy after staining the cells with methylene blue. The cell proliferation study was repeated

three times under identical conditions and three samples were included in each group. The results of the three experiments were combined to compile the final data comprised of a total of nine samples for each treatment group.

2.5. MTT assay

MTT assaying involves a colorimetric measurement based on tetrazolium salt to determine the concentration of living cells. MTT (Sigma, USA) was dissolved in PBS (5 mg/ml) and sterilized by Millipore filtration. After 24, 72, and 120 h of culture, 10 μl of MTT solution was added to each cell-scaffold construct and the controls, and incubated for 2 h in the dark. After careful removal of the medium, 100 μl of di-methyl sulfoxide (Sigma, USA) was added to each well to extract the formazan crystals under gentle shaking. The extract of each sample was transferred to 96-well plate and the absorbance intensities were measured at 570 nm using Biotek Synergy HT Microplate Reader (Biotek, Vermont).

2.6. Tissue formation on functionally graded PCL-β-TCP scaffolds

The functionally graded non-woven composite meshes were electrospun and then were kept under vacuum until use. Typical schematics along with scanning electron micrographs of functionally graded non-woven meshes (punched into 8.6 mm circular discs with 0.35–0.40 mm thickness) are shown in Fig. 1. The ster-ilization and cell culturing procedures were similar to those described in Section 2.4. However, upon culturing in complete medium for 3 days, the medium for the functionally graded scaffolds was replaced with osteogenic differentiation medium, MEM Alpha Medium (Invitrogen, USA), which was further supplemented with fetal bovine serum (Gibco, USA), penicillin/streptomycin (1/0.1/0.01 volume ratio, re-spectively) and $NaHCO_3$ (2.2 g/L). The tissue constructs were harvested after 1 and 4 weeks for histological and biomechanical analyses.

2.7. SEM analysis of tissue constructs

The harvested tissue constructs were fixed in buffered 4% formaldehyde solution and dehydrated using a series of increased concentrations of ethanol, and kept overnight under vacuum. The specimens were then mounted on Al stubs, coated with Au and analyzed using a LEO Gemini 982 scanning electron microscope.

2.8. Histology analysis

The harvested tissue constructs were fixed in buffered 4% formaldehyde solu-tion, dehydrated using a series of graded ethanol solutions (starting with 70% and increasing to 100% ethanol at 10% increments), and embedded in paraffin. Thin cross sections (5 μm) were obtained from the samples embedded in paraffin. The thin sections were stained with hematoxyline and eosin (H&E) to examine the cell distribution and morphology in the constructs. Sections were also stained with Alizarin Red and von Kossa stain for Ca deposition. The stained sections were ana-lyzed using a Nikon Polarizing Microscope (Micron Optics, NJ).

2.9. Biomechanical characterization

Unconstrained uniaxial compression testing of the cultured tissue constructs together with unseeded functionally graded PCL-β-TCP scaffolds were performed using a Rheometric Scientific ARES Rheometer at a constant compression velocity of 0.1 mm/min. Three runs were performed for each sample, and the data were recorded between the strain ranges of 0–10%. The modulus and toughness values of the specimens were determined from the slope of the stress versus strain behavior and the area under the stress versus strain curve, respectively. In order to prevent the drying of tissue constructs during the compression tests, the samples were deformed within a custom designed environmental chamber filled with PBS and kept at 37 °C. The samples were first compressed until a normal force of 0.1 g to assure full contact and the compression tester was zeroed at this level in terms of both the applied stress and the strain and subsequently the compression test was initiated.

2.10. Statistical analyses

Statistical significance was tested by using two-way ANOVA analysis in con-junction with Scheffe's Posthoc test and using SPSS software package. The p levels at which differences between groups were considered statistically significant are de-fined in the captions of the relevant figures.

3. Results and discussion

3.1. Scaffold fabrication and characterization

The application of the hybrid technology to incorporate β-TCP nanoparticles into PCL nanofibers with continuously changing concentrations yielded a highly interconnected and porous 3D matrix with varying concentrations of β-TCP nanoparticles contained in randomly oriented nanofibers (Fig. 1). The process generated nanofibers and fibers in the diameter range of 200–2000 nm, and β-TCP nanoparticle concentrations continuously ranging from zero to 15% by weight. Fig. 1 shows the micro-graphs associated with the top (Fig. 1a,b) and side (Fig. 1c) sections of a typical punctured scaffold, with the well-
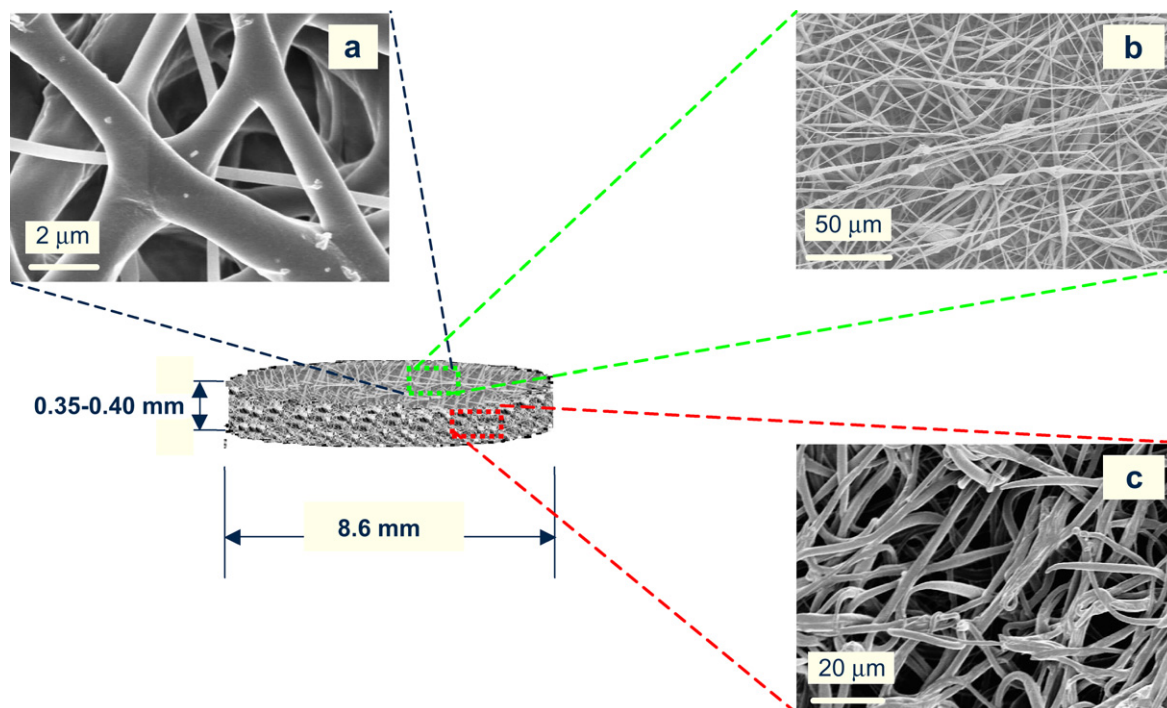
Fig. 1. SEM micrographs from the top (a, b), and side (c) sections of functionally-graded electrospun PCL-β-TCP composite mesh fabricated using an applied potential of 5 kV, distance between the spinneret and the collecting plate of 7.5 cm, flow rate of 10 μl min⁻¹, and spinneret inner diameter of 600 μm.
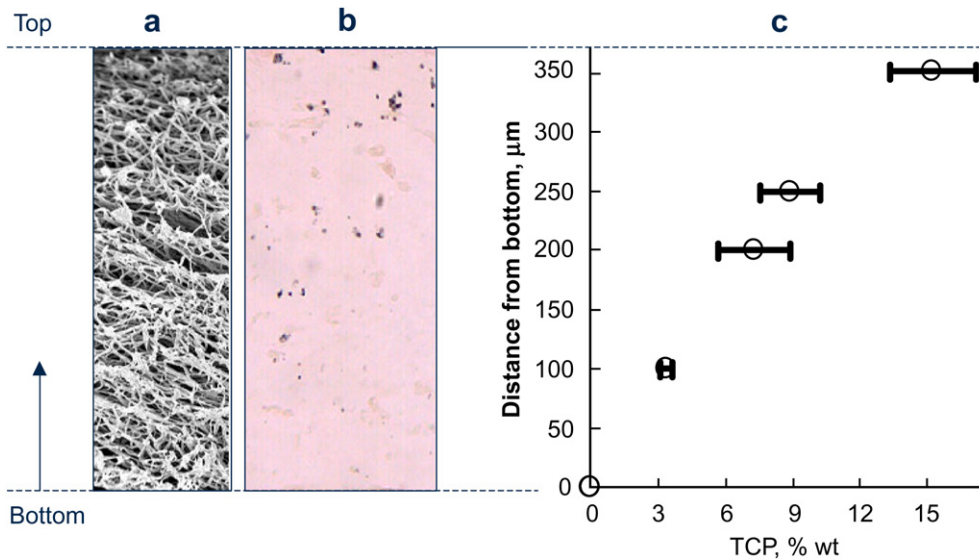
Fig. 2. SEM micrograph of cross-section of the functionally graded non-woven mesh (a), von Kossa staining for distribution of β-TCP nanoparticles along distance (b), and the quantification of β-TCP concentration with TGA (c).

interconnected pores with the sizes ranging between 5 and 50 μm evident.

A typical cross-section of the electrospun functionally graded scaffold is shown in Fig. 2a. The cross-section shows the typical distribution of the fibers and nanofibers located in between the bottom and top surfaces of the scaffold. The distribution of the β-TCP concentration as a function of distance from the bottom surface of the scaffold was determined using time-sectioning followed by thermo-gravimetric analysis, TGA, of specimens located at various distances from the bottom surface. The results of TGA for the compositional distribution of β-TCP nanoparticles as a function of distance away from the bottom surface are shown in Fig. 2c. The concentration of the β-TCP nanoparticles increases from zero at the bottom surface of the scaffold to 15% by weight at the top surface of the scaffold.

The ability to alter the concentration distribution as a function of distance provides the functional-grading ability to our methodology. The β-TCP concentration could be altered in a monotonically increasing fashion as shown in Fig. 2c. The von Kossa staining results shown in Fig. 2b further reveals the gradual change of concentration of β-TCP nanoparticles as a function of distance from the bottom surface of the scaffold. The metallic silver associated with von Kossa staining gives rise to the black spots shown in Fig. 2b. The greater prevalence of the black spots at the top versus the bottom surface of the scaffold is indicative of the increasing Ca concentration associated with the increasing β-TCP nanoparticle concentration as one moves away from the bottom surface. Overall, Fig. 2 indicates that a monotonically increasing gradual distribution of β-TCP nanoparticles as a function of distance could indeed by achieved. It should be noted that by controlling the feeding rates of the individual ingredients into the twin-screw extruder as a function of time, the ultimate distributions of the concentrations of two or multiple ingredients can be controlled generating the requisite functionally graded scaffolds targeting particular tissue engineering applications.

As the concentrations of the ingredients vary as a function of location within the confines of the electrospun meshes, the mechanical properties are expected to change as a function of location also. The distribution of typical mechanical properties obtained upon tensile deformation experiments are shown in Fig. 3. The mechanical properties of the different sections of the functionally

graded meshes located between the bottom and top surfaces and containing differing concentrations of β-TCP were determined. The typical elongation at break values of the PCL, PCL-β-TCP with 6% β-TCP, and PCL-β-TCP with 12% β-TCP meshes were 259, 202 and 171%, respectively, while the tensile stress at break values were 810, 990, and 1080 kPa, respectively. Furthermore, the modulus values, i.e., the slopes of the stress versus elongation curves within the strain limit of elasticity, were determined to be 18.5, 19.5, and 27.5 kPa for the PCL, PCL-β-TCP with 6% β-TCP, and PCL-β-TCP with 12% β-TCP, respectively. These results clearly show the distribution of the mechanical properties as a function of the differing concentrations of β-TCP found at different sections of the graded non-woven electrospun meshes. The distributions of the mechanical properties of the non-woven meshes can be further manipulated by tailoring processing geometries and conditions to obtain varying degrees of dispersion and mixedness, and particle size distribution as well as distributions of concentrations of ingredients upon changes in the operating conditions and the feeding rates into the twin-screw extruder to give rise to any type of desired functional grading of the scaffolds.
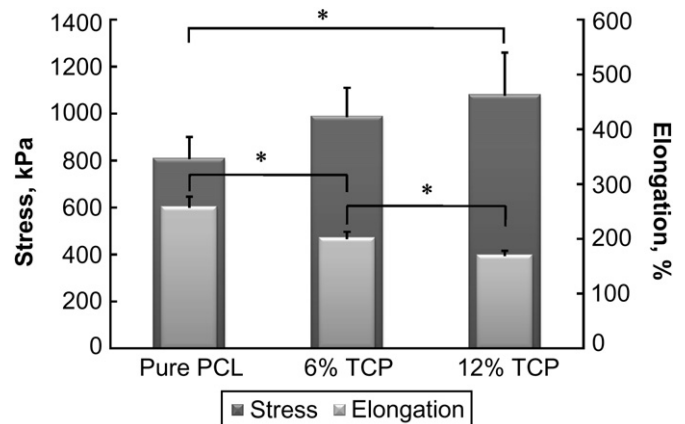
Fig. 3. Mechanical properties of PCL and PCL-β-TCP non-woven meshes with varying β-TCP concentrations. Stress and elongation data correspond to the values at break (* denotes statistical significance with $p < 0.10$).

3.2. Effect of β-TCP on the attachment, proliferation, and differentiation of MC3T3-E1 cells

The cell adhesion behavior and the proliferation rates on the functionally graded scaffolds are important and determine the quality and suitability of the scaffold for the targeted application. In the past, the mouse preosteoblast cells from bone-calvaria (MC3T3-E1) have been extensively used to investigate the change in morphology, bone matrix formation, mineralization, and expression of bone related proteins [30–33]. Generally, the initial cell attachment and a rapid cell division period are followed by a transitional period of formation of type I collagen-rich extracellular matrix. In the final stage achieved after the elapse of approximately 2 weeks upon cell seeding, the expression of bone related proteins and mineral deposition further promote the osteoblastic differentiation [32]. We have also used the mouse preosteoblast cells from bone-calvaria (MC3T3-E1) for our demonstration study.

The typical attachments of the MC3T3-E1 cells to the surfaces of tissue culture plate, pure PCL scaffold, and PCL-β-TCP scaffold with 15% β-TCP, and their morphologies after 24 h are shown in Fig. 4. The MC3T3-E1 cells attach to all of the surfaces tested, however they exhibit different attachment behavior and morphologies when grown on the different surfaces. They adhere and spread well on the tissue culture plate, which was surface modified using corona discharge, and moderately on pure PCL nanofibers and relatively poorly on PCL-β-TCP scaffolds with 15% β-TCP. It was observed in the earlier studies that the presence of nano-indentations, which can also be formed by the nanoparticles on the surfaces of nanofibers as in the case of the present study, or other types of surface irregularities affect the attachment and morphology of osteoblasts and fibroblasts [34–36].

The relatively poor adhesion and spreading of MC3T3-E1 cells on PCL nanofibers incorporated with β-TCP nanoparticles as compared to other surfaces can be attributed primarily to the presence of protrusions created by the β-TCP nanoparticles on the fiber surfaces (see Fig. 2a). It is expected that the height of the protrusions be small and the spacing between the protrusions be large enough to enable the clustering of integrins (around 30 nm in length), which is a requirement for the formation of mature and stable focal adhesions [35]. When the β-TCP nanoparticles (with diameters in the range 50–2500 nm) are highly concentrated on the surfaces of the fibers, the probability of the integrins reaching the surface and eventually to achieve stable focal adhesion gets smaller. The existence of such a structure at the surface of the fibers, therefore, prevents the cell cytoplasm to expand equally well in all directions and thus makes it difficult for the cells to proliferate due to the lack of adequate number of contact points with each other.

As part of this study, the effect of β-TCP nanoparticles on the hydrophilicity of PCL-β-TCP scaffold was also assessed and it was found that incorporation of 15% (by weight) of β-TCP nanoparticles into the PCL fibers decreased the contact angle only slightly from $133°$ to $127°$, suggesting that it is the roughness of the surfaces, associated with the different concentrations of β-TCP nanoparticles which play a more dominant role in the adhesion behavior of the preosteoblast cells.

The effects of β-TCP on the proliferation rates of osteoblast-like MC3T3-E1 [37] and Wistar-rat calvaria osteoblast [38] cells were studied earlier and it was determined that the rate of proliferation of cells in the presence of β-TCP was lower than that on tissue culture plates. As shown in Fig. 5, where the growth rates of MC3T3-E1 cells on tissue culture plates (control), on PCL scaffolds, and on PCL-β-TCP scaffolds containing 15% β-TCP are reported, these earlier findings were corroborated by the results of our study.

Clearly, the proliferation rates of MC3T3-E1 cells on pure PCL scaffolds and PCL-β-TCP scaffolds were lower than that on tissue culture plates at and after 72 h of culture. The difference is significant between the proliferation rate on tissue culture plates and PCL-β-TCP scaffolds at the $p < 0.05$, while it is significant between PCL and PCL-β-TCP scaffolds only at $p < 0.10$. These results imply that β-TCP nanoparticles incorporated into nanofibers would
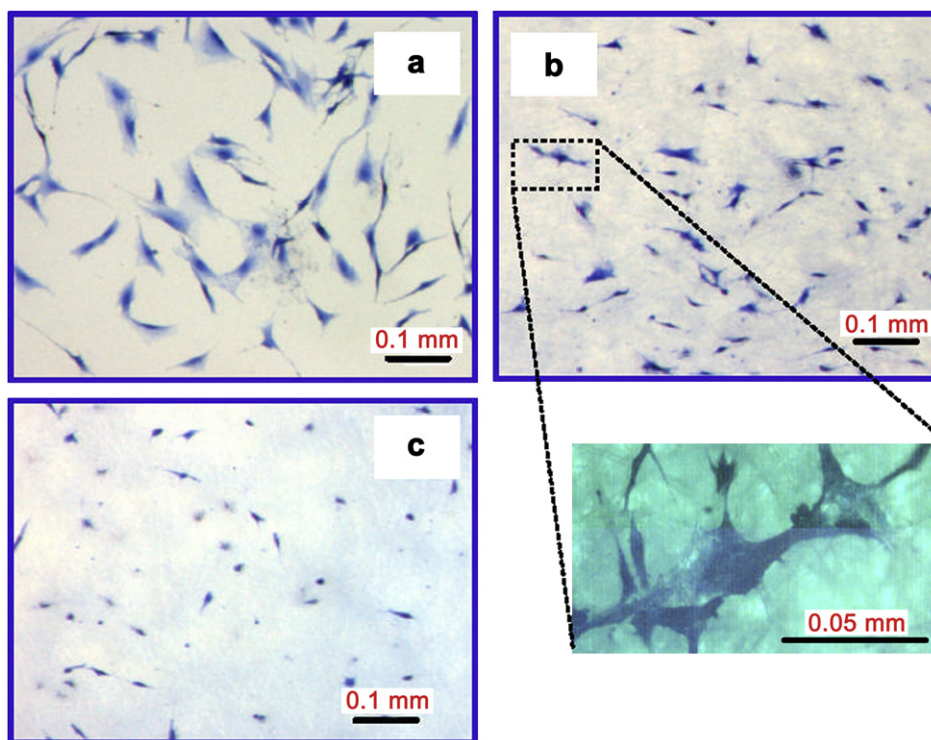
Fig. 4. Attachment and morphology of MC3T3-E1 cells after 24 h on: tissue culture plate (a), on PCL scaffolds (b), and on PCL-β-TCP scaffold containing 15% β-TCP. Scale bar represents 100 μm for a, b, and c, and 50 μm for the inset.
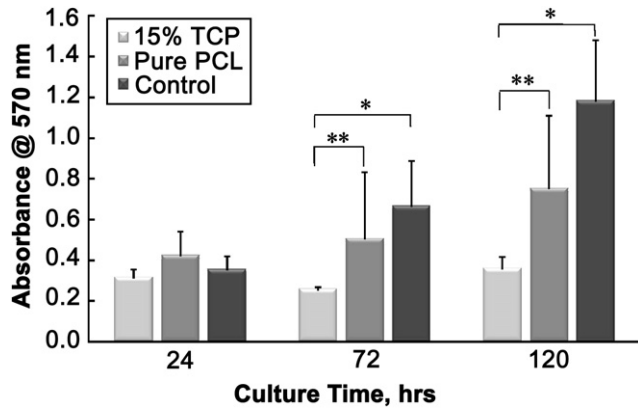
Fig. 5. Comparison of MC3T3-E1 cell proliferation on tissue culture plates (control), PCL scaffolds, and PCL-β-TCP scaffolds containing 15% β-TCP. (* and ** indicate significance with $p < 0.05$, and $p < 0.10$ levels, respectively).

hinder the proliferation of MC3T3-E1 cells, which is in agreement with the previous findings [34]. It was also shown previously that proliferation and differentiation behaviors of osteoblast cells are competing properties, i.e., proliferation rate starts to decrease with the initiation of differentiation [39]. Furthermore, previous experimental studies have revealed that the incorporation of calcium phosphates into the cell culture environment [10,15] and increasing the roughness of the cell culture substrate [40] triggered the expression of typical bone differentiation markers. The lower cell proliferation rates measured on the scaffolds containing 15% β-TCP as compared with pure PCL and control can, therefore, be explained by the accelerated initiation of differentiation process and/or the presence of large protrusions and small spacing between the protrusions created with the incorporation of β-TCP nanoparticles. The characterizations of the cell proliferation and differentiation behavior on our functionally graded scaffolds are discussed next.

The typical scanning electron micrographs of tissue constructs from the functionally graded scaffolds of our study harvested after 1 and 4 weeks of culturing and fixed/dehydrated as described in Section 2.7 are shown in Fig. 6. SEM characterization of the tissue constructs revealed that the period of cell attachment and division was followed by the initiation of collagen synthesis in the extracellular matrix after 1 week and abundant mineralization in the form of Ca deposition after 4 weeks as shown in Fig. 6. At 1 week of culture time, the top surface of the functionally graded scaffold was partially covered with preosteoblast cells initiating collagen synthesis and calcification (Fig. 6a,b). Cells are well spread over the nanofibrous scaffold and the beginnings of a multilayered cell structure were observed. At 4 weeks, the surface was fully covered with multilayers of cells and considerable amount of calcification took place (Fig. 6c). The osteoblastic differentiation process is more visible after 4 weeks, which was marked by the formation of denser collagen bundles with diameters of around 100 nm (Fig. 6e).
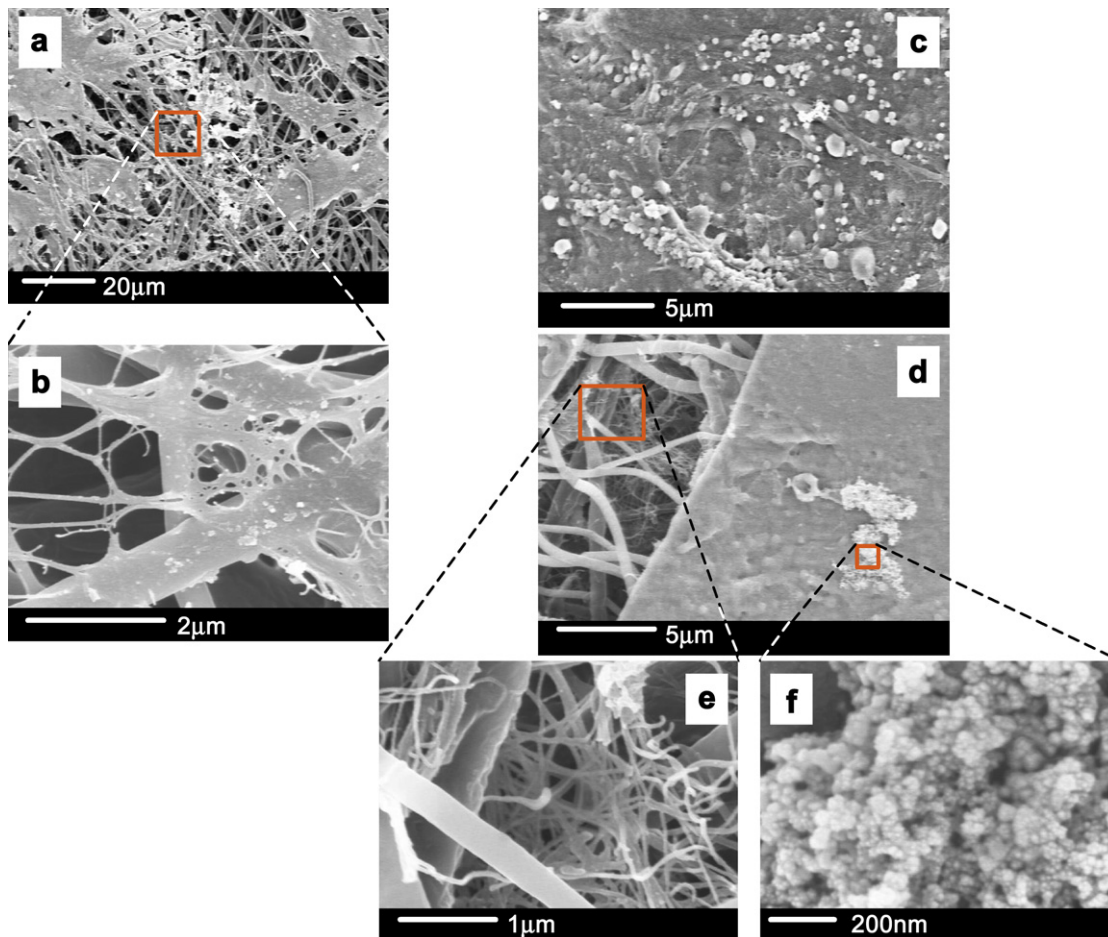
Fig. 6. SEM image of MC3T3-E1 cells seeded on PCL-β-TCP scaffolds. (a) Tissue construct after 1 week of cell culture. The surface of the scaffold is partially covered with osteoblast-like cells. (b) Higher magnification of scaffold surface after 1 week. The spread of cells over the nanofibrous structure and initiation of both Ca deposition and collagen synthesis were observed. (c) Tissue construct after 4 weeks of cell culture. The surface of the scaffold is fully covered with cells. Considerable amount of Ca deposition is noticeable as an indicator of differentiation. (d) Formation of denser collagen bundles and Ca deposition in the bulk of the tissue construct. (e) Higher magnification of the bulk of the tissue with a focus on collagen bundles. (f) Higher magnification of Ca particles deposited by the cells.
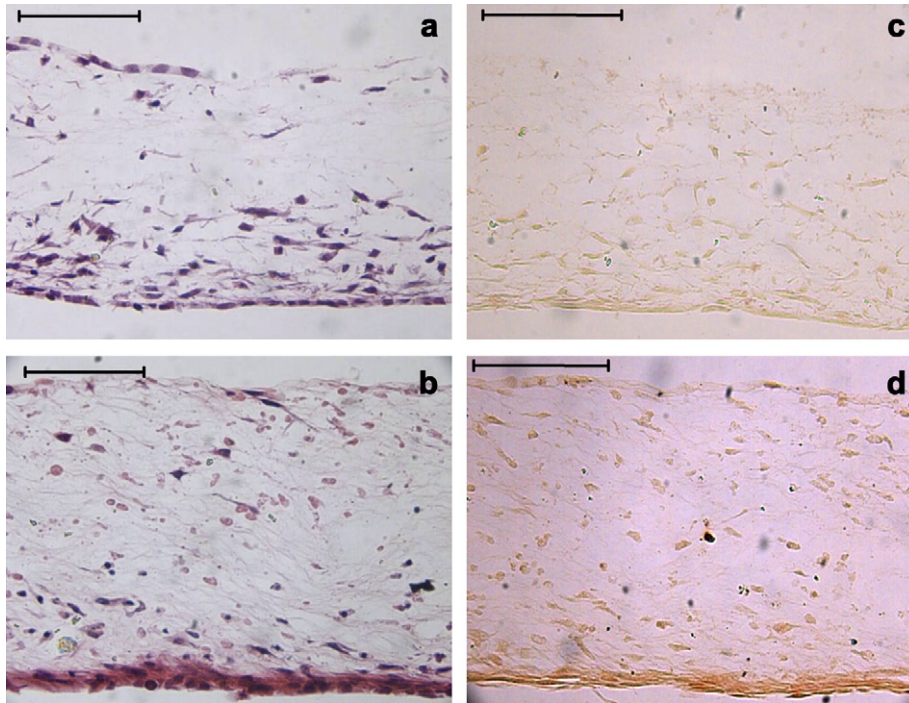
Fig. 7. Light microscopy of tissue constructs: H&E staining after 1 week (a) and after 4 weeks (b), and Alizarin Red staining after 1 week (c) and after 4 weeks (d) of culture. Scale bar is 150 μm.

Significant amounts of Ca deposition were also revealed (Fig. 6f). It is clear from these results that the preosteoblastic MC3T3-E1 cells mostly differentiated into osteoblasts after a series of processes, eventually converting the PCL-β-TCP non-woven composite meshes into a bone tissue-like construct.

3.3. Histological examination of functionally graded tissue samples

The formation of extracellular matrix, synthesis of collagen type-I, and deposition of minerals as indicators of the differentiation activities of bone cells were also verified by histological examination of tissue constructs. H&E staining after 1 week of cell culture revealed the penetration of cells into the interior of the functionally graded scaffolds as shown in Fig. 7a. After 4 weeks of cell culture, a noticeable amount of new ECM was observed in the inter-fiber space across the tissue construct (Fig. 7b). The high surface to volume ratio and the highly interconnected structure of the electrospun scaffold allowed and facilitated the attachment and migration of MC3T3-E1 cells throughout the scaffold to form a 3D extracellular matrix. As the presence of β-TCP nanoparticles was observed to hinder the cell proliferation rate, the scaffolds were placed into the tissue culture plates such that the β-TCP rich side of the functionally graded scaffold is at the bottom, where the cell density is higher during the seeding stage due to the effect of gravity. Unfortunately, we had no means to separate the effect of gravity from these experiments where the cells had a tendency to settle towards the bottom surface during the seeding stage. Such gravitational effects were also observed by others especially when the pore size of the scaffolds is appreciable [41–43]. With time, however, cells migrated upward throughout the scaffold, which became more visible particularly after 4 weeks of cell culture. The very bottom region of the engineered tissue constructs consisted of a thick layer of cells due to presence of extremely high concentration of cells at this portion of the tissue constructs.

The results of Alizarin Red staining after 1 week of cell culture (Fig. 7c) showed the presence of the gradually changing concentration of previously incorporated β-TCP nanoparticles (increasing concentration from top to the bottom). The indication of extra mineral deposition within the scaffold at 1 week of cell culture is rather weak as compared to the concentration of previously incorporated Ca nanoparticles. However, after 4 weeks of cell culture additional mineral deposition by the cells became more evident throughout the tissue constructs as shown in Fig. 7d. The increase in the color intensity of the Alizarin Red stain with time shows the increased bone nodule formation and mineralization both at the surfaces and within the bulk of the tissue constructs. The graded structure of the tissue construct in terms of Ca content is still apparent after 4 weeks of culture. Von Kossa staining of the sections also revealed similar characteristics of the tissue constructs. The tissue constructs generated after 4 weeks of cell culture resemble, in appearance, the bone-cartilage interface in terms of the distribution of the concentration of Ca particles and the associated spatial variation of mechanical properties as well as the
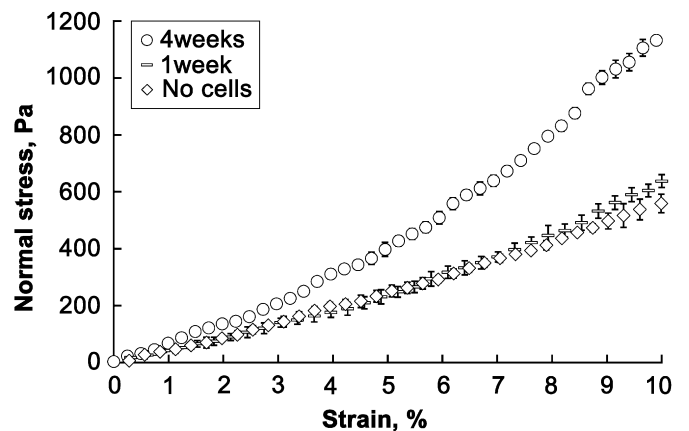
Fig. 8. Biomechanical compression of PCL-β-TCP unseeded scaffolds and tissue constructs after 1 and 4 weeks. The error bars represent the upper and lower bounds determined at 95% confidence level. The narrower error bars are hidden behind the markers for some of the data points.

extracellular matrix formed by the cells migrated into the bulk of scaffold. The gradations observed in the tissue constructs develop as a consequence of the gradations in composition available in the electrospun scaffolds.

3.4. Biomechanical characterization

The compressive stress–strain behavior of engineered tissue constructs after 1 and 4 weeks of culture period, together with the unseeded PCL-β-TCP scaffolds are shown in Fig. 8. The results show that the mechanical properties of the tissue constructs alter significantly after 4 weeks as compared to those after 1 week of cell culture and unseeded scaffolds. The normal stresses in compression determined at 10% strain observed for the unseeded scaffold, the tissue constructs cultured for 1, and 4 weeks were 590, 630, and 1150 Pa, respectively. The insignificant difference between the stress values obtained for unseeded scaffold and the tissue construct cultured for 1 week suggests that only minor changes in the composition and/or structure of cell-seeded scaffold occur after 1 week of cell culturing. However, significant changes in mechanical properties occurred upon the elapsing of 4 weeks as the formation of a bone-like structure progressed.

Previous research suggested that biomechanical properties such as modulus and toughness of bone tissue are good predictors for the degree of mineralization and collagen type-I formation, respectively [44,45]. The modulus and the toughness of the tissue constructs as well as the unseeded scaffolds were determined and the results are shown in Fig. 9. Fig. 9a shows that the modulus of the tissue constructs after 1 and 4 weeks of cell culturing are significantly (at $p < 0.05$) higher than that of unseeded scaffold. In other words, significant but only modest mineralization took place within 1 week of cell culturing while significant and relatively high degree of mineral density was present after 4 weeks. These findings suggest that the mineral deposition was initiated at a time that is earlier than 1 week and that the mineral deposition progressed rapidly during the 4 weeks of cell culture period. Fujihara et al. [15] and Wutticharoenmongkol et al. [46] have also observed similar behavior of mineral deposition by MC3T3-E1 cells on electrospun PCL scaffolds incorporated with functional nanoparticles of $CaCO_3$ or hydroxyapatite.

Fig. 9b shows that the toughness values of the tissue construct cultured for 1 week are slightly higher (but not significant at $p < 0.05$) than those of the unseeded scaffold. The toughness values of the tissue constructs cultured for 4 weeks, however, are significantly (at $p < 0.05$) higher than those of the unseeded scaffolds and the tissue constructs cultured for 1 week. These findings again reinforce the noted penetration of the cells into the interior of the scaffold and the associated development of the expression of bone related proteins at 1 week to form the collagenous extracellular matrix throughout the scaffold. The expression of collagen type-I by MC3T3-E1 cells as a marker of osteoblastic differentiation was also observed by Choi et al. [31] within 10 days of cell culture in tissue culture plates.

4. Conclusions

Functionally graded nanocomposite structure of PCL-β-TCP was fabricated by using a hybrid twin-screw extrusion electrospinning process and its potentials for tissue engineering in general, and to bone-cartilage interface formation in particular were demonstrated using MC3T3-E1 cells. The ability to incorporate the β-TCP nanoparticles into PCL nanofibers in a controlled manner enabled the better mimicking of the compositional and structural characteristics of the bone tissue particularly at the bone-cartilage interface. The approach demonstrated here offers additional degrees of freedom in the engineering of graded constructs for tissue engineering applications.

Fig. 9. Modulus (a) and toughness (b) of the tissue constructs and unseeded scaffolds. (* and ** indicate significance at $p < 0.05$, and $p < 0.1$ levels, respectively).

References

[1] Sasaki N, Sudoh Y. X-ray pole figure analysis of apatite crystals and collagen molecules in bone. Calcified Tissue Int 1997;60:361–7.
[2] Zizak I, Roschger P, Paris O, Misof BM, Berzlanovich A, Bernstorff S, et al. Characteristics of mineral particles in the human bone/cartilage interface. J Struct Biol 2003;144:208–17.
[3] Boyde A, Jones SAJ, Aerssens J, Dequeker J. Mineral density quantitation of the human cortical iliac crest by backscattered electron image analysis: variations with age, sex, and degree of osteoarthritis. Bone 1995;16:619–27.
[4] Bradley DA, Luthuvelu P, Ellis RE, Green EM, Attenburrow D, Barrett R, et al. Characterisation of mineralisation of bone and cartilage: X-ray diffraction and Ca and Sr K_α X-ray fluorescence microscopy. Nucl Instrum Meth B 2007; 263:1–6.
[5] Vacanti A, Vacanti JP. Bone and cartilage reconstruction with tissue engineering approaches. Otolaryngol Clin North Am 1994;27:263–76.
[6] Reddi AH. Role of morphogenetic proteins in skeletal tissue engineering and regeneration. Nat Biotechnol 1998;16:247–52.
[7] Hutmacher DW. Scaffolds in tissue engineering bone and cartilage. Biomaterials 2000;21:2529–43.

[8] Rose FRAJ, Oreffo ROC. Bone tissue engineering: hope vs hype. Biochem Biophys Res Commun 2002;292:1–7.

[9] Shin M, Yoshimoto H, Vacanti JP. In vivo bone tissue engineering using mesenchymal stem cells on a novel electrospun nanofibrous scaffold. Tissue Eng 2004;10:33–41.

[10] Ehara A, Ogata K, Imazato S, Ebisu S, Nakano T, Umakoshi Y. Effects of α-TCP and TetCP on MC3T3-E1 proliferation, differentiation and mineralization. Biomaterials 2003;24:831–6.

[11] Zhou Y, Hutmacher DW, Varawan SL, Lim TM. In vitro bone engineering based on polycaprolactone and polycaprolactone-tricalcium phosphate composites. Polym Int 2006;56:333–42.

[12] Kim HW, Song JH, Kim HE. Nanofiber generation of gelatin-hydroxyapatite biomimetics for guided tissue regeneration. Adv Funct Mater 2005;15: 1988–94.

[13] Degirmenbasi N, Kalyon DM, Birinci E. Biocomposites of nanohydroxyapatite with collagen and poly(vinyl alcohol). Colloid Surface B 2006;48:42–9.

[14] Wutticharoenmongkol P, Sanchavanakit N, Pavasant P, Supaphol P. Novel bone scaffolds of electrospun polycaprolactone fibers filled with nanoparticles. J Nanosci Nanotechnol 2006;6:514–22.

[15] Fujihara K, Kotaki MS, Ramakrishna S. Guided bone regeneration membrane made of polycaprolactone/calcium carbonate composite nano-fibers. Biomaterials 2005;26:4139–47.

[16] Dror Y, Salalha W, Khalfin RL, Cohen Y, Yarin AL, Zussman E. Carbon nanotubes embedded in oriented polymer nanofibers by electrospinning. Langmuir 2003;19:7012–20.

[17] Ko F, Gogotsi Y, Ali A, Naguib N, Ye H, Yang GL, et al. Electrospinning of continuous carbon nanotube-filled nanofiber yarns. Adv Mater 2003;15:1161–5.

[18] Weinand C, Pomerantseva I, Neville CM, Gupta R, Weinberg E, Madisch I, et al. Hydrogel-β-TCP scaffolds and stem cells for tissue engineering bone. Bone 2006;38:555–63.

[19] Chew SY, Wen J, Yim EKF, Leong KW. Sustained release of proteins from electrospun biodegradable fibers. Biomacromoecules 2005;6:2017–24.

[20] Mikos AG, Herring SW, Ochareon P, Elisseeff J, Lu HH, Kandel R, et al. Engineering complex tissues. Tissue Eng 2006;12:3307–39.

[21] Catledge SA, Clem WC, Shrikishen N, Chowdhury S, Stanishevsky AV, Koopman M, et al. An electrospun triphasic nanofibrous scaffold for bone tissue engineering. Biomed Mater 2007;2:142–50.

[22] Schaefer D, Martin I, Shastri P, Padera RF, Langer R, Freed LE, et al. In vitro generation of osteochondral composites. Biomaterials 2000;21:2599–606.

[23] Gao J, Dennis JE, Solchaga LA, Awadallah AS, Goldberg VM, Caplan AI. Tissue-engineered fabrication of an osteochondral composite graft using rat bone marrow-derived mesenchymal stem cells. Tissue Eng 2001;7:363–71.

[24] Spalazzi JP, Doty SB, Moffat KL, Levine WN, Lu HH. Development of controlled matrix heterogeneity on a triphasic scaffold for orthopedic interface tissue engineering. Tissue Eng 2006;12:3497–508.

[25] Thomas V, Catledge SA, Vohra YK. Functionally graded electrospun scaffolds with tunable mechanical properties for vascular tissue regeneration. Biomed Mater 2007;2:224–32.

[26] Zhao DM, Wang YX, Xu RW, Wu G, Zhang LQ, Yu DS. Composition-graded films of fluoroapatite/PHB fabricated via electrospinning for tissue engineering. J Bioact Compat Pol 2007;22:379–93.

[27] Erisken C, Kalyon DM, Wang H. A hybrid twin screw extrusion/electrospinning method to process nanoparticle-incorporated electrospun nanofibers. Nanotechnology 2008;19:165302.

[28] Kalyon DM, Malik M. An integrated approach for numerical analysis of coupled flow and heat transfer in co-rotating twin screw extruders. Int Polym Proc 2007;22:293–302.

[29] Tang H, Kalyon DM. Unsteady circular tube flow of compressible polymeric liquids subject to pressure-dependent wall slip. J Rheol 2008;52:507–26.

[30] Hurley MM, Abreu C, Harrison JR, Lichtler AC, Raisz LG, Kream BE. Basic fibroblast growth factor inhibits type I collagen gene expression in osteoblastic MC3T3-E1 cells. J Biol Chem 1993;268:5588–93.

[31] Choi JY, Lee BH, Song KB, Park RW, Kim IS, Sohn KY, et al. Expression patterns of bone-related proteins during osteoblastic differentiation in MC3T3-El cells. J Cell Biochem 1996;61:609–18.

[32] Wenstrup RJ, Fowlkes JL, Witte DP, Florer JB. Discordant expression of osteoblast markers in MC3T3-E1 cells that synthesize a high turnover matrix. J Biol Chem 1996;271:10271–6.

[33] Yoshimoto H, Shin YM, Terai H, Vacanti JP. A biodegradable nanofiber scaffold by electrospinning and its potential for bone tissue engineering. Biomaterials 2003;24:2077–82.

[34] Dalby MJ, Riehle MO, Sutherland DS, Agheli H, Curtis ASG. Morphological and microarray analysis of human fibroblasts cultured on nanocolumns produced by colloidal lithography. Eur Cell Mater 2005;9:1–8.

[35] Kunzler TP, Huwiler C, Drobek T, Vörös J, Spencer ND. Systematic study of osteoblast response to nanotopography by means of nanoparticle-density gradients. Biomaterials 2007;28:5000–6.

[36] Degirmenbasi N, Ozkan S, Kalyon DM, Yu X. Surface patterning of poly (L-lactide) upon melt processing: in vitro culturing of fibroblasts and osteoblasts on surfaces ranging from highly crystalline with spherulitic protrusions to amorphous with nanoscale indentations. J Biomed Mater Res A 2008; doi: 10.1002/jbm.a.31874.

[37] Aoki S, Yamaguchi S, Nakahira A, Suganuma K. Preparation of porous calcium phosphates using a ceramic foaming technique combined with a hydrothermal treatment and the cell response with incorporation of osteoblast-like cells. J Ceram Soc Japan 2004;112:193–9.

[38] Sun JS, Tsuang YH, Liao CJ, Liu HC, Hang YS, Lin FH. The effects of calcium phosphate particles on the growth of osteoblasts. J Biomed Mater Res 1997;37: 324–34.

[39] Owen TA, Aronow M, Shalhoub V, Barone LM, Wilming L, Tassinari MS. Progressive development of the rat osteoblast phenotype in vitro reciprocal relationships in expression of genes associated with osteoblast proliferation and differentiation during formation of the bone extracellular matrix. J Cell Physiol 1990;143:420–30.

[40] Liao H, Andersson AS, Sutherland D, Petronis S, Kasemo B, Thomsen P. Response of rat osteoblast-like cells to microstructured model surfaces in vitro. Biomaterials 2003;24:649–54.

[41] Nehrer S, Breinan HA, Ramappa A, Young G, Shortkroff S, Louie LK, et al. Matrix collagen type and pore size influence behaviour of seeded canine chondrocytes. Biomaterials 1997;18:769–78.

[42] O'Brien FJ, Harley BA, Yannas IV, Gibson LJ. The effect of pore size on cell adhesion in collagen-GAG scaffolds. Biomaterials 2005;26:433–41.

[43] Zeltinger J, Sherwood JK, Graham DA, Mueller R, Griffith LG. Effect of pore size and void fraction on cellular adhesion, proliferation, and matrix deposition. Tissue Eng 2001;7:557–72.

[44] Garnero P, Borel O, Gineyts E, Duboeuf F, Solberg H, Bouxsein M, et al. Extracellular post-translational modifications of collagen are major determinants of biomechanical properties of fetal bovine cortical bone. Bone 2006;38:300–9.

[45] Burr DB. The contribution of the organic matrix to bone's material properties. Bone 2002;31:8–11.

[46] Wutticharoenmongkol P, Pavasant P, Supaphol P. Osteoblastic phenotype expression of MC3T3-E1 cultured on electrospun polycaprolactone fiber mats filled with hydroxyapatite nanoparticles. Biomacromolecules 2007;8:2602–10.